Can the Southern Hemisphere annular mode affect China winter monsoon?

Zhiwei Wu,[1,2] Jianping Li,[1] Bin Wang,[2] and Xinhua Liu[3]

Received 20 November 2008; revised 8 April 2009; accepted 14 April 2009; published 5 June 2009.

[1] Many previous studies suggested that the anomalous Northern Hemisphere annular mode (NAM) and associated low boundary forcing (e.g., snow cover) greatly influence the China winter monsoon (CWM) variability on interannual to inter-decadal timescales. In this article, it is found that the Southern Hemisphere annular mode (SAM) also well correlates with the two observed CWM major modes, which has not been revealed before. Note that the two CWM major modes are obtained by performing Empirical Orthogonal Function (EOF) analysis on winter surface air temperature at 160 gauge stations across China for the 1951–2006 period. They explain around 70% of the total CWM variances. The first EOF mode exhibits a homogeneous spatial pattern with the corresponding principal component displaying a significant inter-decadal variation, which reflects the warming trend in China during the past 56 years. The second EOF mode shows a meridional seesaw pattern and is basically associated with significant interannual variations. Both of the leading modes are intimately associated with the simultaneous SAM-like hemispheric circulation anomalies. Moreover, the SAM-like anomalies signal precursory conditions for the first CWM mode in boreal autumn. The relevant physical mechanisms by which anomalous autumn SAM may affect the CWM are investigated with NCAR Community Atmospheric Model version 3 (CAM3). When SAM is in a strong phase during boreal autumn, the circum-Antarctic upper level jet stream displaces poleward and the corresponding surface wind speeds reduce in the region between 45°S and 30°S, inducing a hemispheric-scale warm sea surface temperature (SST) belt beneath. Such an anomalously warm SST belt persists through boreal winter and weakens the Hadley cell. The weakened Hadley cell in boreal winter corresponds to anomalous southerlies prevailing in the lower troposphere over China, which favor a weak CWM. The intimate linkage between the autumn SAM and CWM may be instrumental for understanding interactions between the Northern and Southern Hemisphere and can provide a way to predict the CWM variations.

Citation: Wu, Z., J. Li, B. Wang, and X. Liu (2009), Can the Southern Hemisphere annular mode affect China winter monsoon?, *J. Geophys. Res.*, *114*, D11107, doi:10.1029/2008JD011501.

1. Introduction

[2] The China winter monsoon (CWM) is a principal component of the East Asian winter monsoon (EAWM) which is believed to be the strongest winter monsoon system on the Earth due to the huge thermal contrast between the world's largest landmass (the Eurasian continent) and its largest ocean basin (the Indo-Pacific Ocean) [e.g., *Li*, 1955; *Tao*, 1957; *Ding*, 1994; *Chang et al.*, 2006]. It influences not only the local circulation and climate but also the North America even the global climate through changing positions of the tropical heat sources and convergence centers and teleconnections [e.g., *Chang and Lau*, 1982; *Lau and Chang*, 1987; *Yang et al.*, 2002; *Wang and Li*, 2004]. When the CWM breaks out, it is usually associated with an intense drop in air temperature, gales, snowfalls and freezing weather conditions [e.g., *Ji et al.*, 1997]. The 2008 peculiar snow storm in southern China led to billions of dollars worth property losses and hundreds of civilian deaths.

[3] Many previous studies suggested that the CWM is highly relevant to the Northern Hemisphere large-scale circulation anomalies, i.e., the Northern Hemisphere annular mode (NAM) or Arctic Oscillation (AO) [e.g., *Gong and Wang*, 1999; *Gong et al.*, 2001; *Wu and Wang*, 2002; *Li and Wang*, 2003a; B. Wang et al., Another look at climate variations of the East Asian winter monsoon: Northern and southern temperature modes, submitted to *Journal of Climate*, 2009, hereinafter referred to as Wang et al., submitted manuscript, 2009]. Observational analysis by *Gong et al.* [2001] suggested that the NAM (or AO) may influence the CWM through its impact on the Siberian High. A negative NAM phase is concurrent

[1]State Key Laboratory of Numerical Modeling for Atmospheric Sciences and Geophysical Fluid Dynamics, Institute of Atmospheric Physics, Chinese Academy of Sciences and Graduate School of the CAS, Beijing, China.
[2]Department of Meteorology and IPRC, University of Hawaii, Honolulu, Hawaii, USA.
[3]National Meteorological Center, China Meteorological Administration, Beijing, China.

Copyright 2009 by the American Geophysical Union.
0148-0227/09/2008JD011501

with a stronger East Asian Trough and an anomalous anticyclonic flow over the Urals at the middle troposphere (500 hPa). The Eurasian low boundary forcing may also affect the CWM variations [e.g., *Clark and Serreze*, 2000; *Zhu et al.*, 2000; Wang et al., submitted manuscript, 2009]. *Jhun and Lee* [2004] suggested that there are two major domains whose snow cover correlates well with the Northern Hemisphere large-scale circulation anomalies in preceding autumn. One is Siberian High region and the other is Northeast China and far eastern Russia. This is supported by general circulation model simulations, which showed that extensive snow cover induces a stronger than normal Aleutian Low and Siberian-Mongolian High, enhanced East Asian jet, and colder lower troposphere, and leads to a stronger winter monsoon [e.g., *Watanabe and Nitta*, 1998, 1999; *Kumar and Yang*, 2003; *Gong et al.*, 2003]. This snow cover effect was also shown in the midlatitude East Asian winter monsoon mode by Wang et al. (submitted manuscript, 2009). Over all, previous studies basically focus on impacts of the *Northern Hemisphere* circulation anomalies and the associated low boundary forcing anomalies on the CWM.

[4] The Southern Hemisphere annular mode (SAM) is the NAM's counterpart in the Southern Hemisphere. It is a seesaw phenomenon between the sea level high-pressure belt across Chile and Argentina and the low-pressure area of Weddell Sea and the Bellingshausen Sea and has great influences on the Southern Hemisphere climate [e.g., *Walker*, 1928; *Kidson*, 1975; *Rogers and van Loon*, 1982; *Cai et al.*, 1999; *Cai and Watterson*, 2002; *Li et al.*, 2005; *Yuan and Li*, 2008]. SAM reflects hemispheric-wide fluctuations in air mass between two annular belts of action over middle and high latitudes similar to what the NAM does [e.g., *Thompson and Wallace*, 2000a, 2000b; *Li and Wang*, 2003a]. *Trenberth et al.* [2004] investigated the interannual variability of patterns of global atmospheric mass and found that the dominant global monthly variability overall is associated with the SAM, which is active in all months of the year, while the NAM is the third most important pattern. Some studies already revealed that the preceding SAM anomalies may lead to some climate anomalies in the Northern Hemisphere. *Nan and Li* [2003] found that there is a significantly positive correlation between the boreal spring SAM and the following summer monsoon rainfall in the middle and lower reaches of the Yangtze River. *Xue et al.* [2003] also noticed interannual variations of Mascarene High and Australian High are significantly related to the following East Asian summer monsoon rainfall.

[5] Then, can the SAM affect the CWM, and if so, how does it work? To address these issues, it is important to first elaborate the fundamental characteristics of the major modes of the CWM (see section 3). In section 4, the relationship between the SAM and the major modes is discussed, as well as that between the NAM and the major modes for comparison. On the basis of these results, possible physical mechanisms have been investigated (see section 5). In the last section, the main conclusions are summarized and some outstanding issues are discussed.

2. Data, Model and Methodology

[6] The main data sets employed in this study include surface air temperature (Ts) at 160 gauge stations across China for the 1951–2006 period, the improved Extended Reconstructed SST Version 2 (ERSST V2 [*Smith and Reynolds*, 2004]), sea level pressure (SLP) from the University of East Anglia/Climatic Research Unit (CRU [*Jones*, 1987]) and the European Center for Medium-Range Weather forecast (ECMWF) 40 years reanalysis data [ERA-40 [*Uppala et al.*, 2005]), the National Center for Environmental Prediction/Department of Energy reanalysis (NCEP-2 henceforth) data [*Kanamitsu et al.*, 2002]. The NAM index (NAMI) and SAM index (SAMI) are taken from *Li and Wang* [2003a] and *Nan and Li* [2003]. The reason we choose these two indices is because their definitions are more simplified and well reflect the basic features of the SAM and NAM documented in previous studies [*Rossby*, 1939; *Lorenz*, 1951; *Kutzbach*, 1970; *Wallace and Gutzler*, 1981]. The NAMI is defined as the normalized difference in zonal-averaged SLP anomalies between 35°N and 65°N, while the SAMI is defined as the normalized difference in zonal-averaged SLP anomalies between 40°S and 65°S. Winter and autumn in this article refer to boreal season and are defined as December, January and February (DJF), and September, October and November (SON), respectively.

[7] The atmospheric general circulation model (AGCM) used in this study is the NCAR Community Atmospheric Model version 3 (CAM3). The horizontal resolution is T42 (approximately 2.8° longitude × 2.8° latitude), with 26 hybrid vertical levels. (A complete description of this model version is available online at http://www.ccsm.ucar.edu/models/atm-cam/docs/description/.)

[8] In this study, raw winter (DJF) Ts at 160 gauge stations across China [*Wu et al.*, 2006b] for the 1951–2006 period is used to derive the major modes of the CWM with Empirical Orthogonal Function (EOF) analysis. The winter monsoon is also called cold surge [e.g., *Chang et al.*, 1983] and Ts is the most fundamental variable associated with the EAWM [e.g., *Li*, 1955; *Tao*, 1957; *Ding*, 1994; Wang et al., submitted manuscript, 2009]. Although topographic difference may result in significant local variations on the seasonal reversal of winds and annual variation of rainfall in the EAWM domain [e.g., *Ramage*, 1971; *Matsumoto*, 1992; *Hamada et al.*, 2002; *Li and Zeng*, 2002; *Chang et al.*, 2004], the Ts variation is always the same, namely, a strong winter monsoon corresponding to cold Ts and a weak winter monsoon corresponding to warm Ts (Wang et al., submitted manuscript, 2009).

[9] Combination of ERA-40 and NCEP-2 data sets is adopted to get a longer time period (1957–2006) (Wang et al., submitted manuscript, 2009). The combination is conducted with following steps: For the 1957–2001 period, ERA-40 data are adopted; for the 2002–2006 period, NCEP-2 data are adopted but with some modifications of adding climatology difference (NCEP2 minus ERA-40) to 2002–2006 NCEP-2 data. The motivation is to remove the climatology difference between ERA-40 and NCEP-2 data sets. To verify the validity of the combination data, we compared the EOF analysis results between the CRU (not shown) and combination of ERA-40 and NCEP-2 and found the spatial patterns which have observations are similar and their principal components are also of the same variability. Therefore a combination of ERA-40 and NCEP-2 is adopted in this study, ultimately.

3. Major Modes of the CWM

[10] The two leading CWM modes (hereafter EOF1 and EOF2) account for 57.1%, 12.2% of the total variance,

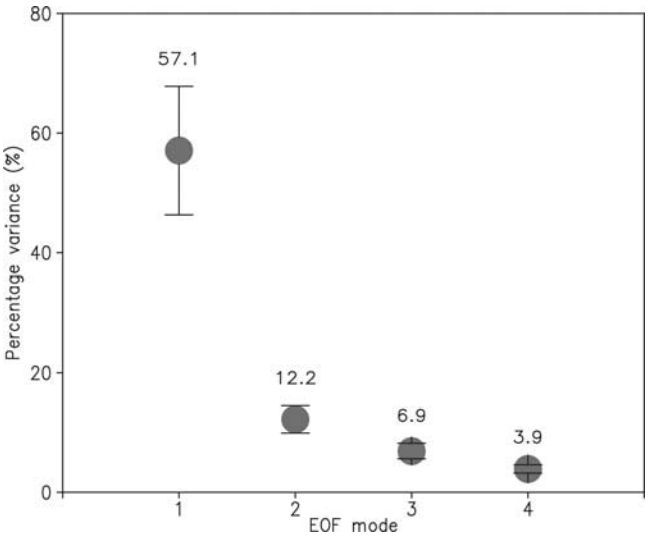

Figure 1. Fractional variance (%) explained by the first four EOF modes of winter (December–February, hereafter DJF) air temperature at 160 gauge stations across China for the 1951–2006 period and the associated unit standard deviation of the sampling errors.

respectively (Figure 1). The fractional (percentage) variances of the first four eigenvectors and the associated unit standard deviation of the sampling errors are all shown in Figure 1. According to the rule given by *North et al.* [1982], EOF1 and EOF2 modes are statistically distinguished from each other and the rest of the eigenvectors in terms of the sampling error bars (Figure 1). The sum of the explained variance of the two leading modes reaches 69.3%. Thus the CWM variability is dominated by these two leading modes. They may represent the predictable part of the CWM [e.g., *Wang et al.*, 2008; *Wu and Li*, 2008]. Seasonal prediction of these two leading modes may be the principal aspect of the CWM seasonal prediction.

[11] The spatial pattern of EOF1 mode shows a homogeneous pattern, which indicates the Ts in China has the same sign of variability, with two extreme value centers located over North China and Northwest China, respectively (Figure 2a). The corresponding principal component (PC) (hereafter PC1) has a significant increasing trend (exceeding 95% confidence level) (Figure 2b). These manifest that it is relatively colder before 1980s and warmer after 1980s in China and the warming trend is relatively larger in North and Northwest China than that in the southern China. EOF1 mode basically reflects the warming trend over China during the period 1951–2006. This warming pattern was also shown in other studies [e.g., *Wu et al.*, 2006a].

[12] EOF2 mode primarily shows a meridional dipole spatial pattern. Negative Ts anomalies primarily prevail over the region north of 40°N, and positive Ts anomalies control the continent south of 40°N (Figure 2c). Their extreme value centers are located at Northeast China and South China, respectively. The principal component of EOF2 mode (hereafter PC2; Figure 2d) does not show an obvious warming trend but considerable interannual variations. This mode mainly reflects the Ts seesaw effect between the northern and southern China.

[13] In fact, these two major modes are corresponding to two different trajectories of cold air mass influencing China [e.g., *Li*, 1955; *Tao*, 1957; Wang et al., submitted manuscript, 2009]. EOF1 mode denotes the middle and eastern trajectory, which can influence majority of China, yet with a decreasing trend in the past fifty years. EOF2 mode represents the

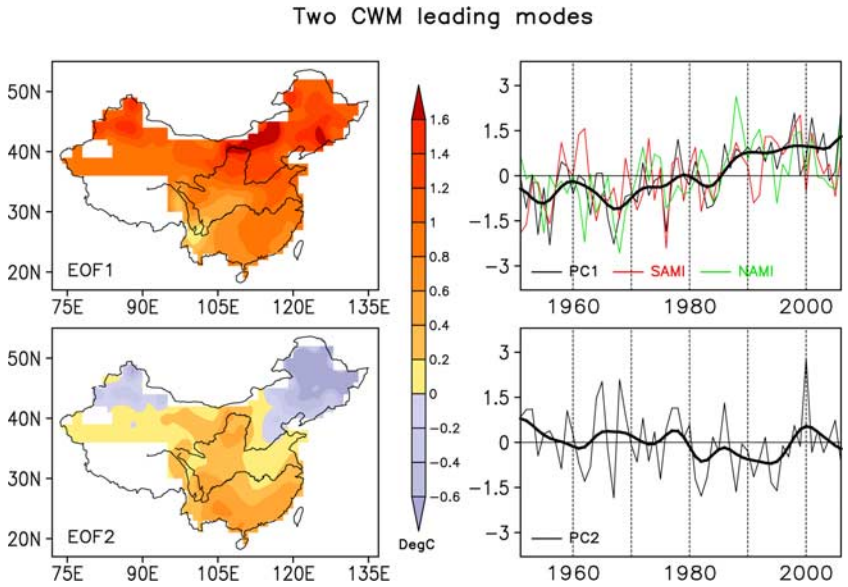

Figure 2. Spatial patterns (EOFs) (color shadings in Figures 2a and 2c, unit of DegC) and principal components (PCs) (contours in Figures 2b and 2d) of the two leading EOF modes in Figure 1. The bold line represent decadal variation obtained using a 9-point Gaussian-type filter. The red and green curves in Figure 2b represent the Southern Hemisphere annular mode index (SAMI) and the Northern Hemisphere annular mode index (NAMI) time series, respectively.

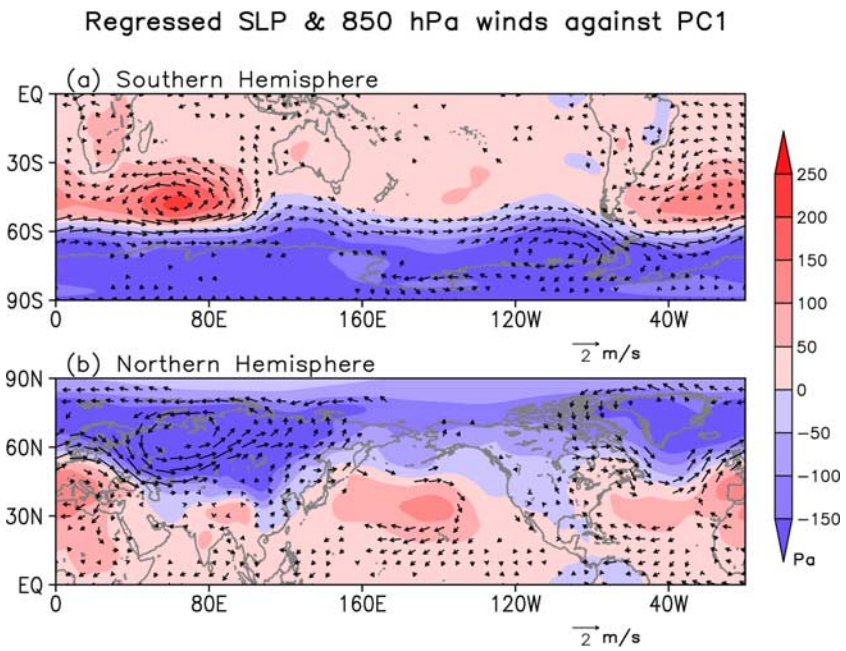

Figure 3. DJF sea level pressure (SLP) anomalies (color shadings, unit of Pa) and 850 hPa wind anomalies (vectors, unit of m s^{-1}) over the (a) Southern Hemisphere and (b) Northern Hemisphere, which were linearly regressed against the PC1 in Figure 2.

western cold air mass trajectory, which basically impacts on southern China.

4. SAM (NAM) Anomalies Associated With the CWM

[14] EOF1 mode is highly relevant to the simultaneous SAM and NAM, associated with correlation coefficients between PC1 and SAMI (NAMI) reaching 0.55 (0.55) (Figure 2). Both exceed the 99% confidence level based on the Student *t*-test. If we decompose PC1 into an interannual (IA) and inter-decadal (ID) component, namely,

$$\mathrm{PC1} = \mathrm{PC1(IA)} + \mathrm{PC1\,(ID)}$$

The IA component contains all Fourier harmonics that have periods less than 8 years, while the ID component contains all Fourier harmonics that have periods longer than 8 years. The correlation coefficients between the SAMI (NAMI) and PC1 (ID) reach 0.62 (0.62), while those between the SAMI (NAMI) and PC1 (IA) are 0.29 (0.3). It indicates that the high correlation between the simultaneous SAM (NAM) and the CWM dominant mode is primarily contributed by the decadal-trend timescale. We regressed raw SLP and 850 hPa winds onto PC1 to show the low-level circulation anomalies associated with the EOF1 mode. It can be clearly seen from Figure 3a that there is a tremendous negative SLP anomaly center over the mid-high latitudes between 60°S and 90°S, associated with large areas of cyclonic wind anomalies around the South Pole region at 850 hPa. There are two positive SLP centers over South Atlantic and South Indian Ocean, respectively, associated with 850 hPa anticyclonic wind anomalies. This pattern reflects a typical positive SAM phase as documented by *Thompson and Wallace* [2000a, 2000b]. Similar features exist in the Northern Hemisphere, large areas of negative SLP anomalies covering over the high latitudes between 45°N and 90°N, centered at the Eurasian continent and North Atlantic (Figure 3b). Cyclonic wind anomalies prevail over the Eurasian and Greenland at 850 hPa. Two positive SLP anomaly centers cover central North Pacific and North Atlantic−western Europe, which are relatively weak compared with its Southern Hemisphere counterpart. It basically exhibits a positive NAM phase pattern [e.g., *Thompson and Wallace*, 2000a, 2000b; *Trenberth et al.*, 2004].

[15] EOF2 mode better correlates with the simultaneous SAM than with the NAM, associated with correlation coefficients between PC2 and SAMI (NAMI) reaching −0.33 (−0.27) beyond 95% (90%) confidence level. In the Southern Hemisphere, a pronounced positive SLP anomaly belt controls the South Pole region, accompanied by a remarkable negative SLP anomaly belt that covers the midlatitudes between 30°S and 60°S (Figure 4a). The Northern Hemisphere has a more complicated circulation pattern than the Southern Hemisphere does (Figure 4b). The North Pole region is basically controlled by positive SLP anomalies and a remarkable negative SLP center extends from North Atlantic to the western Europe, which basically exhibits a negative North Atlantic Oscillation (NAO) pattern [*Rogers*, 1984; Figure 4b]. As a matter of fact, the correlation coefficient between PC2 and NAO index [*Li and Wang*, 2003b] is −0.35, exceeding the 99% confidence level based on the Student *t*-test.

[16] Figure 5 and Figure 6 show the midlevel and high-level circulation anomalies associated with the two major EOF modes. For EOF1 mode, 500 hPa geo-potential height anomalies and 200 hPa wind anomalies have similar spatial patterns in both the Southern Hemisphere and Northern

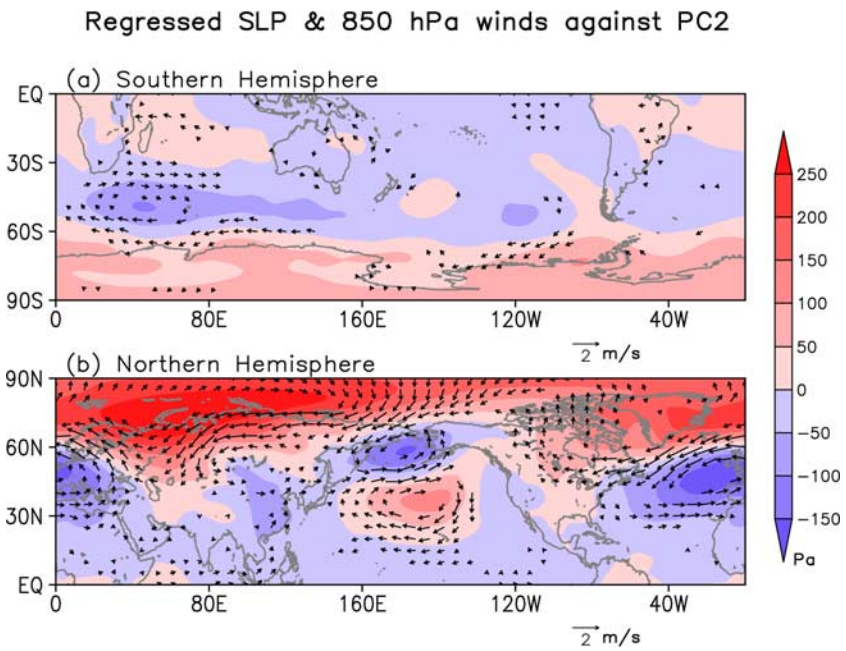

Figure 4. Same as Figure 3 except for PC2.

Hemisphere (Figure 5) with those of the lower level (Figure 3), which manifests that the large-scale SAM-like atmospheric anomalies associated with EOF1 mode have an equivalent barotropic structure in the troposphere. As for EOF2 mode, the Southern Hemisphere also displays a similar pattern in the upper troposphere (Figure 6a) with that in the lower troposphere (Figure 3a), so does the North Atlantic domain (Figure 6b). It indicates that the SAM-like and NAO-like anomalies associated with the EOF2 mode bear an equivalent barotropic structure in the troposphere. In addition, a tremendous 500 hPa low center associated with 200 hPa cyclonic wind anomalies covers the Siberian region and expands to the north of 60°N (Figure 6b), which generates an enhanced baroclinic pattern.

[17] Figure 7 shows the lead-lag correlation map between PC1 (PC2) and SAMI (NAMI) time series from Mar(0) to Oct(1). Here "0" denotes the simultaneous year and "1" denotes the following year. Mar(0) leads the simultaneous winter (D(0)J(1)F(1)) by 9 months. The preceding SAM signal (Figure 7b) is stronger and more stable than the preceding

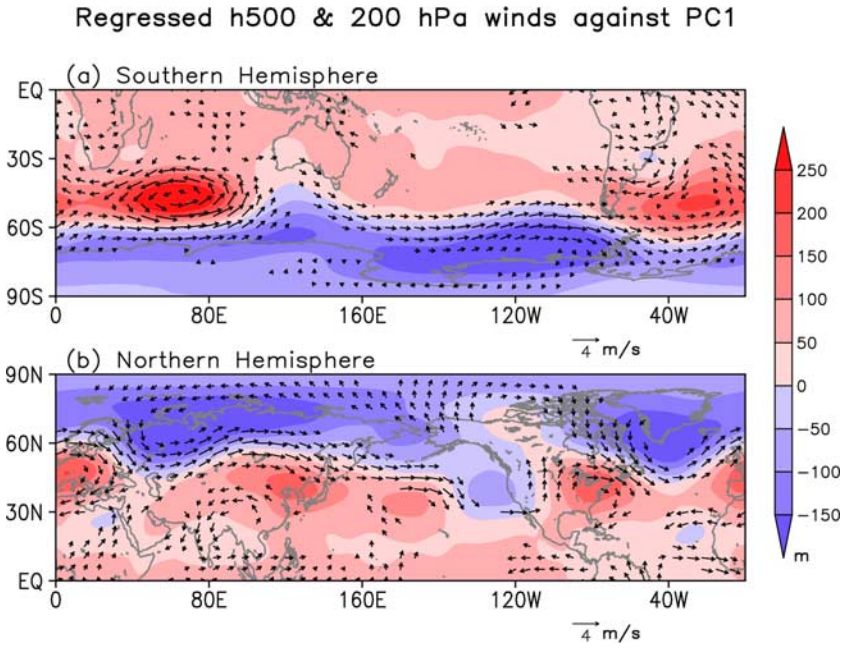

Figure 5. DJF 500 hPa geo-potential height anomalies (color shadings, unit of m) and 200 hPa wind anomalies (vectors, unit of m s^{-1}) over the (a) Southern Hemisphere and (b) Northern Hemisphere, which were linearly regressed against the PC1 in Figure 2.

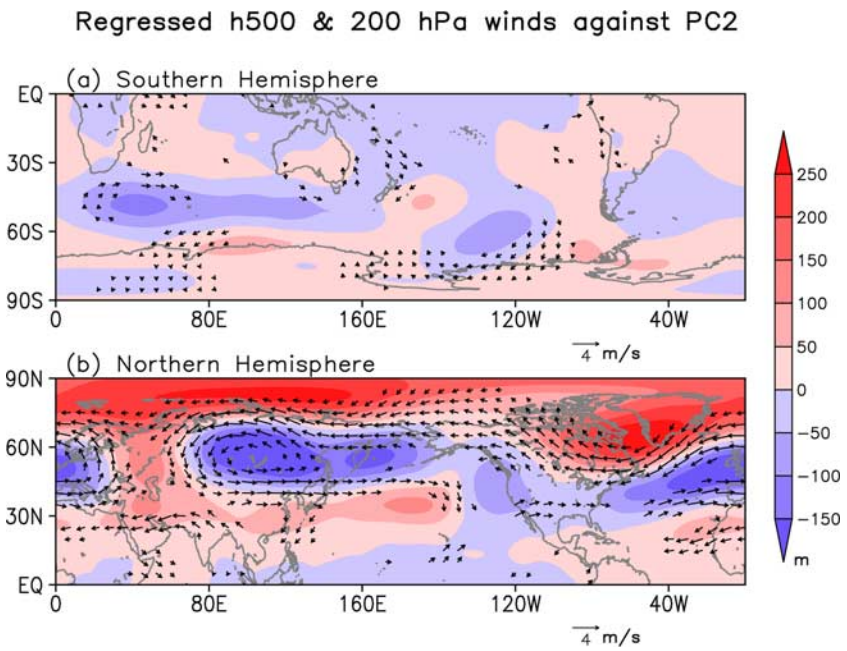

Figure 6. Same as Figure 5 except for PC2.

NAM signal (Figure 7a) with the two CWM major modes. The SAM provides significant precursory conditions from Aug(0) and persists till the following year in terms of EOF1 mode. Thus the SAM yields a strong and durative connection with the CWM leading mode, which makes it of seasonal prediction value. Note that although the NAM has a good simultaneous relationship with the EOF1 mode, it does not have a durative leading relationship with the EOF1 mode. In contrast to the strong lead-lag correlation with the EOF1 mode, the SAM weakly correlates with the EOF2 mode, only with simultaneous relationship exceeding the 95% confidence level based on Student *t*-test. The NAM is also weakly correlated with the EOF2 mode.

[18] From the above analysis, both of the leading modes are associated with simultaneous SAM-like hemispheric circulation anomalies and the SAM anomalies associated with the first CWM mode are more stable and durative than the NAM anomalies. However, the statistical relationship between the SAM and CWM does not warrant any cause and effect.

5. Physical Mechanisms

[19] As noted above that the SAM anomalies associated with the first CWM mode are more stable and durative than the NAM anomalies, the following will focus on how the SAM anomalies can affect the first CWM mode. The significant relationship between the SAM and the first CWM mode starts from preceding autumn (Figure 7b). Since the atmosphere (or SAM), on its own, lacks the mechanisms to generate predictable variations, potential predictability of such fluctuations can arise only from coupled mechanisms that involve low boundary forcing such as SST [*Namias*, 1959, 1965]. To understand how boreal autumn SAM anomalies affect SST variations, first investigated are surface wind speed anomalies associated with autumn SAM. Note that strong (weak) SAM is usually corresponding to the poleward (equatorward) displacement of high-level jet streams around the Antarctic [e.g., *Thompson and Wallace*, 2000a, 2000b]. Because of the equivalent-baratropic structure of the SAM (Figures 3a and 5a) [e.g., *Thompson and Wallace*, 2000a, 2000b; *Trenberth et al.*, 2004], the surface wind speed varies in phase with high-level jet stream. Figure 8 shows the lead-lag correlations between global zonal 10-m wind speed with autumn SAMI. The most notable feature is a

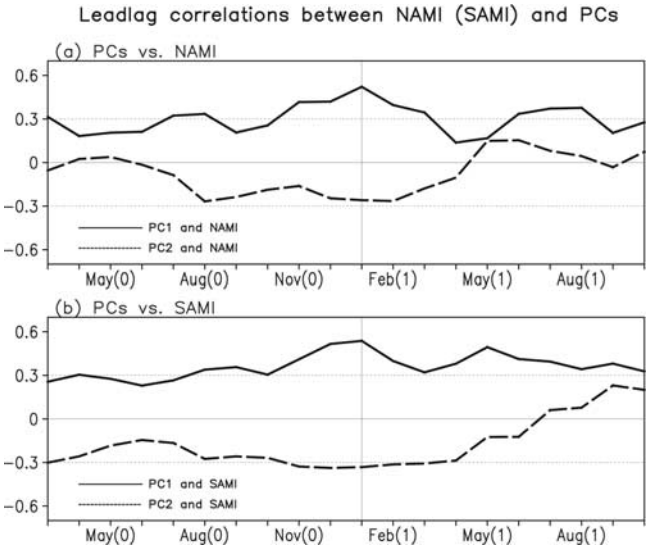

Figure 7. The lead-lag correlation coefficients between the two leading PCs and the NAMI (SAMI) time series. The vertical line indicates Jan(1) where the simultaneous correlations are shown. The two black dotted lines represent 95% confidence level based on Student *t*-test. (a) PCs and the NAMI. (b) PCs and the SAMI.

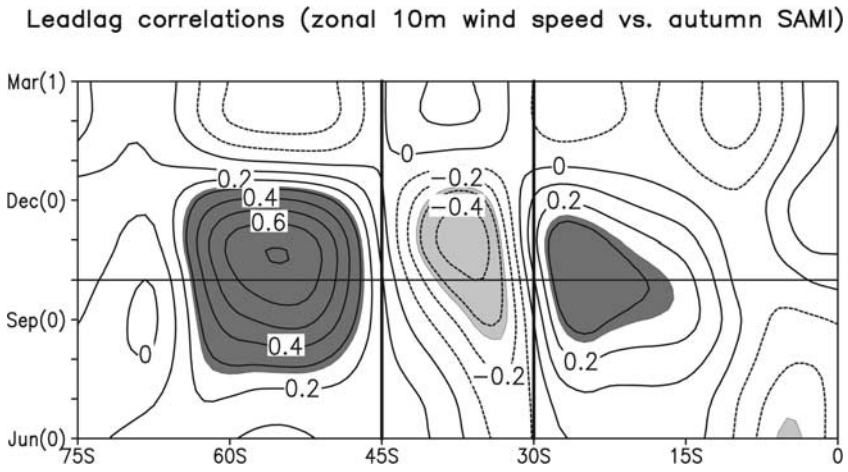

Figure 8. The lead-lag correlation coefficients between the autumn SAMI and global zonal mean 10-m winds speed from Jun(0) to Mar(1). The vertical line indicates Oct(0) where the simultaneous correlations are shown. The shaded areas represent 95% confidence level.

dipole correlation pattern sustaining from Aug(0) through Dec(0) in the Southern Hemisphere mid-high latitudes (south of 30°S): positive correlation south of 45°S and negative correlation within 45°S–30°S. It indicates that the strong SAM in boreal autumn is usually associated with high surface wind speed south of 45°S and low wind speed within 45°S–30°S, and *vice versa*. This is basically due to displacement of jet streams around the Antarctic when anomalous SAM occurs in boreal autumn. Since high (low) sea surface wind speed often favors cold (warm) SST anomalies by latent heat flux exchange, corresponding to this dipole surface wind speed pattern, SST exhibits a similar pattern (negative correlations near the polar and equatorial regions, and positive correlations in the Southern Hemisphere middle latitudes), yet the positive correlation within 45°S–30°S is dominant (Figure 9). The positive correlation between the autumn SAMI and the SST within 45°S–30°S persists from autumn through winter, which manifests that strong SAM autumn will induce anomalously warm SST within 45°S–30°S sustaining through boreal winter.

[20] Figure 10 displays DJF composite SST difference between high and low autumn SAMI years (high minus low SAMI years). Note that a high (low) SAMI is measured by one standard deviation. SST basically exhibits a seesaw pattern in the Southern Hemisphere mid-high latitudes (south of 30°S), a warming belt between 45°S and 30°S and a cooling belt between 70°S and 50°S, which is primarily consistent with implication from Figure 8. The warming belt between 45°S and 30°S is more pronounced compared to the cooling belt, which is also in favor of the result from Figure 9. There are four warming SST centers located at the South Indian Ocean, South Atlantic Ocean, southwestern Pacific, and southeastern Pacific, respectively. To quantitatively describe such a warming SST belt in the Southern Hemisphere, a zonal SST index (ZSSTI) is defined as the global zonal mean SST averaged in the region (45°S–30°S) during boreal winter.

[21] To further investigate large-scale DJF atmospheric circulation anomalies associated with such a hemispheric-scale warm SST belt, DJF simultaneous correlation is com-

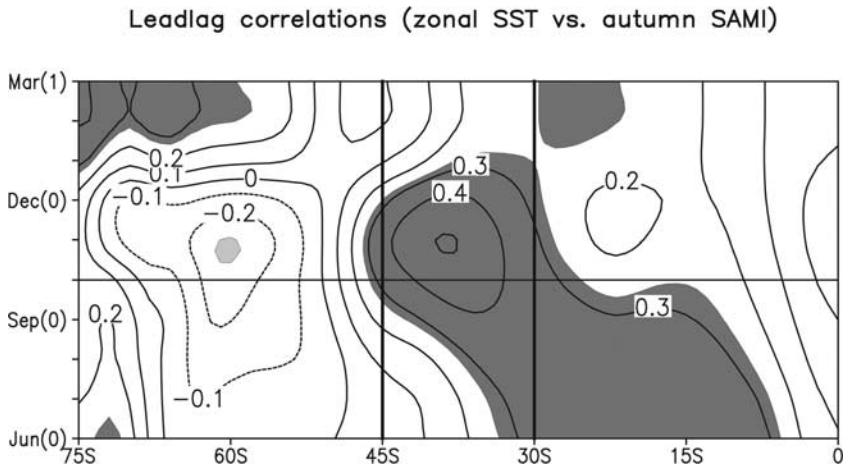

Figure 9. The lead-lag correlation coefficients between the autumn SAMI and global zonal mean SST from Jun(0) to Mar(1). The bold horizontal line indicates Oct(0) where the simultaneous correlations between the PCs and SST are shown. The shaded areas represent 95% confidence level.

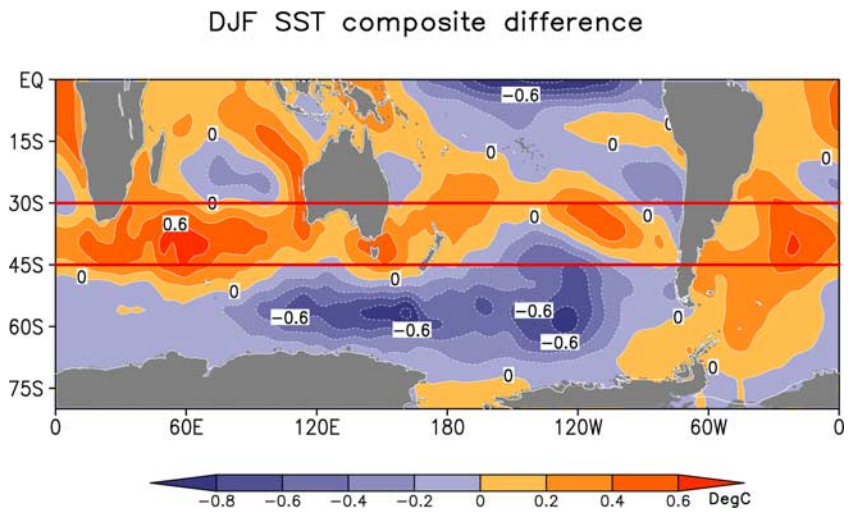

Figure 10. DJF SST composite difference between high and low autumn SAMI (high minus low). A high (low) SAMI is measured by one standard deviation. The global zonal mean SST between the two red lines (45°S–30°S) is defined as a zonal SST index (ZSSTI).

puted between the ZSSTI and global (East Asian) zonal mean vertical (meridional) velocities (Figure 11). In boreal winter, the climatological upward branch of global zonal mean Hadley cell prevails over the equatorial region (15°S–10°N) (dark shadings in Figure 11a), two downward branches primarily located in the Southern Hemisphere (45°S–30°S) and Northern Hemisphere (15°N–35°N), respectively. During the high ZSSTI DJF, warm SST anomalies within (45°S–30°S) usually excite upward movements, which weakens the downward branch of the Hadley cell

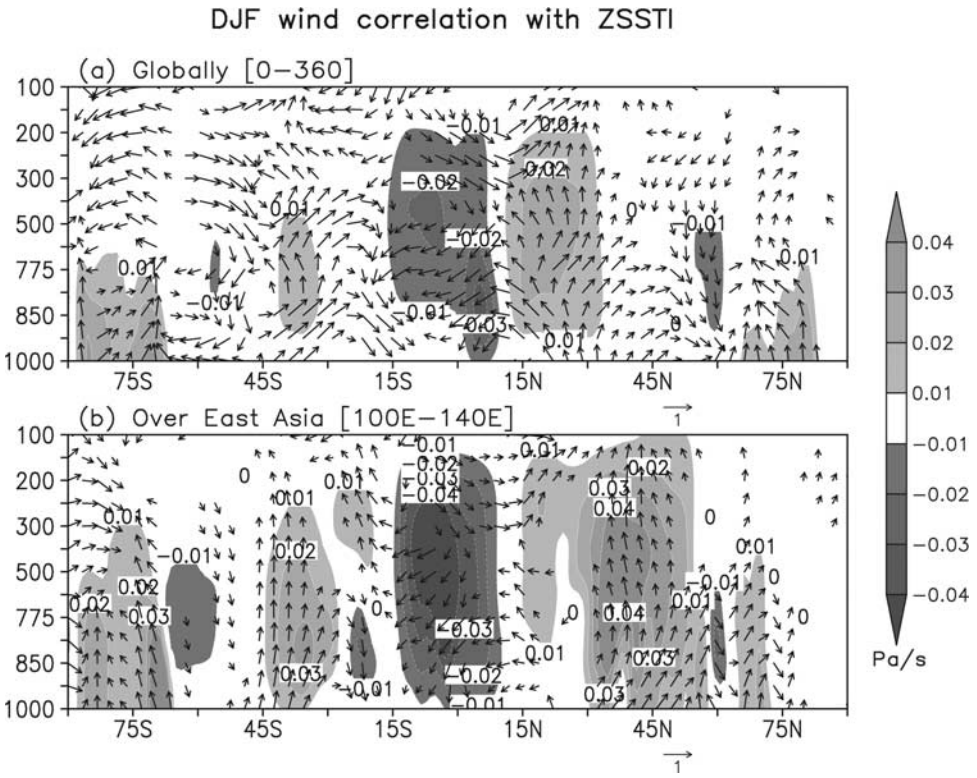

Figure 11. Vector correlation map of DJF meridional wind section averaged (a) globally (0°–360°) and (b) over East Asia (100°E–140°E) with reference to ZSSTI defined in Figure 10. The vertical and meridional components of the vectors represent, respectively, the correlation coefficients of the vertical and meridional winds with ZSSTI. The shaded areas denote the climatological mean of zonal mean vertical velocity. The dark (light) shadings correspond to upward (downward) movements (contours in units of Pa/s). The vector correlation shown in Figure 11 exceeds 95% confidence level.

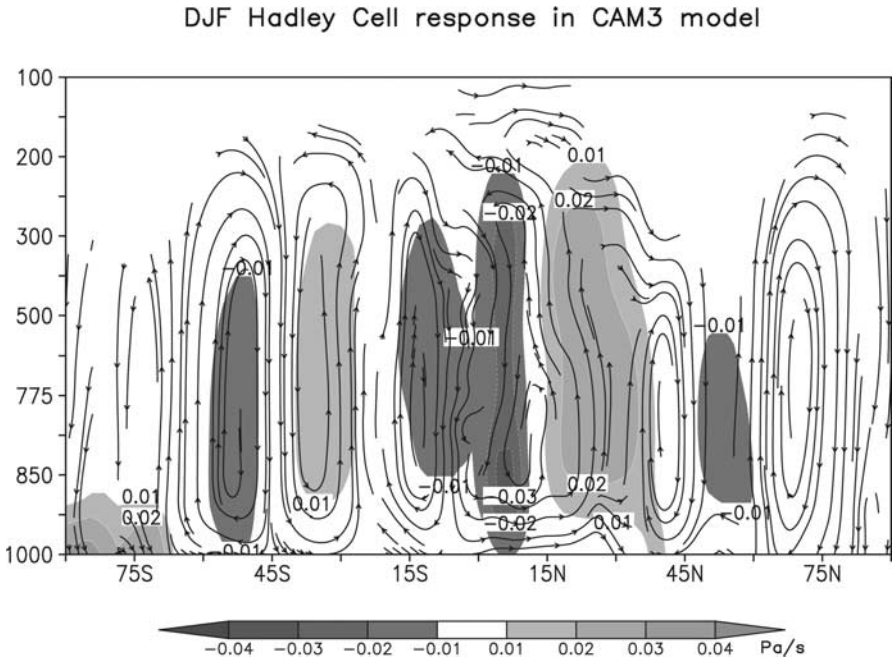

Figure 12. DJF globally averaged Hadley Cell response to a high ZSSTI forcing in the CAM3 model. The shaded areas denote the climatological mean of zonal mean vertical velocity. The dark (light) shadings correspond to upward (downward) movements (contours in units of Pa/s).

(see vector correlations within 45°S–30°S in Figure 11a) and further weakens the Hadley cell in the Southern Hemisphere. Since the Hadley cells in the two hemispheres share the same upward branch, the weakening of the Southern Hemisphere Hadley cell will lead to the weakening of its counterpart in the Northern Hemisphere (see vector correlations within 15°N–35°N; Figure 11a). In such cases, the lower troposphere in the Northern Hemisphere is corresponding to southerly wind anomalies.

[22] Similar features exist in the zonal mean Hadley cell over the East Asian sector (Figure 11b). The global strongest Hadley cell in boreal winter is located in the East Asia because of the huge meridional thermal contrast [e.g., *Li*, 1955; *Tao*, 1957; *Ding*, 1994; *Chang et al.*, 2006], therefore, the upward branch (within 15°S–10°N) and two downward branches of the Hadley cell (within 45°S–30°S and 15°N–52.5°N) over East Asia (shadings in Figure 11b) are stronger and wider than those of the global zonal mean (shadings in Figure 11a). Because of the warm SST anomalies within (45°S–30°S), the Hadley cell over the domain (100°E–140°E) is also weakened with upward anomalies within (45°S–30°S) and (15°N–52.5°N) and downward anomalies within 15°S–10°N. The lower troposphere in (15°N–52.5°N) is controlled by southerly wind anomalies which are usually considered to be a weak CWM [e.g., *Ding*, 1994; *Chang et al.*, 2006; *Wu et al.*, 2006a].

[23] To further verify the above assumption on how the DJF warm SST anomalies within (45°S–30°S) influence the Hadley Cell, we performed numerical experiments with the CAM3 model described in section 2. The control run was integrated for 12 years and the last 10 years' integration was used to derive a reference state. The sensitivity test was integrated for 10 years. The 10-year integrations were used to construct a 10-member ensemble (arithmetic) mean to reduce the uncertainties arising from differing initial conditions. To isolate and mimic the impacts of SST warming, the only difference between the control and sensitivity experiments is 1°C increasing in SST over the (45°S–30°S) region in the sensitivity run. It can be clearly seen from Figure 12 that warm SST anomalies within (45°S–30°S) usually excite ascending anomalies, which weakens the downward branch of the Hadley cell, and further weakens the Hadley cell in the Southern Hemisphere. Because the Hadley cells in the two hemispheres share the same upward branch, the weakening of the Southern Hemisphere Hadley cell will lead to the weakening of its counterpart in the Northern Hemisphere and the prevailing of southerly wind anomalies in the lower troposphere in the Northern Hemisphere.

6. Summary and Discussion

[24] The 2008 extreme snow storm event which occurred in China triggered fervent attention to the CWM research. In this study, two CWM major modes are obtained by performing EOF analysis on winter surface air temperature at 160 gauge stations across China for the 1951–2006 period. They explain around 70% of the total CWM variances. EOF1 mode exhibits a homogeneous spatial pattern with the PC1 displaying a significant inter-decadal variation, which reflects the warming trend in China during the past 56 years. EOF2 mode shows a meridional seesaw pattern and is basically associated with interannual variations. Previous studies have noticed that the CWM is highly relevant to the Northern Hemisphere large-scale circulation systems such as the NAM [e.g., *Gong et al.*, 2001; *Wu and Wang*, 2002; *Li and Wang*, 2003a]. According to the results in this study, the SAM simultaneously correlates well with both of the two CWM leading modes. The linkage between the SAM and

the first CWM mode is even more stable and durative in terms of lead-lag correlation. These have not been revealed before.

[25] The SAM yields another source of predictability for the CWM. The main difficulty in understanding the influences of the SAM on the Northern Hemisphere climate is how SAM signals can propagate from the Southern Hemisphere into the Northern Hemisphere. *Thomas and Webster* [1994] suggested that wave propagation from the Southern Hemisphere into the Northern Hemisphere will most likely be observed when the westerly duct is open. In light of the intimate connection between the ENSO and SAM variability [*L'Heureux and Thompson*, 2006], ENSO is also likely to be the implicit link between the SAM and CWM. Some other studies more believed that the influence of SAM was basically transmitted through the "ocean bridges" of Indian Ocean circulation changes [e.g., *Nan and Li*, 2005; *Nan et al.*, 2008]. Evidences provided in this study show that the SAM anomalies playing important roles in affecting the strength of the Hadley cell. When strong (weak) SAM anomalies occur in boreal autumn, the poleward (equatorward) displacement of high-level jet streams yields low (high) surface wind speed anomalies in the region (45°S–30°S) which may induce hemispheric-scale warm (cold) sea surface temperature (SST) belt in this region. Such an anomalous SST pattern persists from boreal autumn through boreal winter and can weaken (strengthen) the Hadley cells in both hemispheres in boreal winter. The weakened (enhanced) Hadley cell is always corresponding to anomalous southerlies (northerlies) prevailing over China in the lower troposphere which favor a weak (strong) CWM. In such cases, the autumn SAM anomalies are tied to the CWM variations.

[26] This work focuses on boreal autumn SAM anomalies. Figure 7 seems to suggest that the SAM's influence on PC1 extends right through to the next boreal autumn. Why is this case? In addition, why does the NAMI & PC1 correlation (Figure 7a) dip below and then above the 95% confidence level leading into the boreal summer? In other seasons, can the SAM trigger similar large-scale circulation anomalies? Under a global warming circumstance, how will the SAM-CWM link change? These issues need further investigations. The results in this work are based on the seasonal mean timescale. Many climate extreme events are of a subseasonal timescale. How well can the SAM contribute to prediction of the subseasonal events? Moreover, since the NAM (NAO) and ENSO are also highly relevant to CWM (e.g., Wang et al., submitted manuscript, 2009), are there any interactions among the NAM, ENSO and SAM during the CWM season? Does this suggest a link between the NAM and the SAM? Why does the SAM have a better correlation with the CWM during the preceding months than the NAM does? These are still outstanding issues which need further investigations. Because of the discrepancy of the reanalysis data in reflecting the Southern Hemisphere, more observation data should be used to accurately quantify the SAM variations [*Marshall*, 2003].

[27] **Acknowledgments.** The authors thank the three reviewers for helpful comments. Jianping Li and Zhiwei Wu acknowledge the support of the 973 program (2006CB403600) and the National Natural Science Foundation of China (grant 40605022 and 40523001). Bin Wang and Zhiwei Wu are supported by NSF climate dynamics program (ATM03-29531) and in part by IPRC, which is in part sponsored by FRCGC/JAMSTEC, NASA, and NOAA.

References

Cai, W., and I. G. Watterson (2002), Modes of interannual variability of the Southern Hemisphere circulation simulated by the CSIRO climate model, *J. Clim.*, *15*, 1159–1174.

Cai, W., P. G. Baines, and H. B. Gordon (1999), Southern mid- to high-latitude variability, a zonal wavenumber 3 pattern, and the Antarctic Circumpolar Wave in the CSIRO coupled model, *J. Clim.*, *12*, 3087–3104.

Chang, C. P., and K. M. Lau (1982), Short-term planetary-scale interaction over the tropics and midlatitudes during northern winter. Part I: Contrast between active and inactive periods, *Mon. Weather Rev.*, *110*, 933–946.

Chang, C. P., J. E. Millard, and G. T. J. Chen (1983), Gravitational character of cold surges during winter MONEX, *Mon. Weather Rev.*, *111*, 293–307.

Chang, C. P., Z. Wang, J. Ju, and T. Li (2004), On the relationship between western maritime continent monsoon rainfall and ENSO during northern winter, *J. Clim.*, *17*, 665–672.

Chang, C. P., Z. Wang, and H. Hendon (2006), The Asian winter monsoon, in *The Asian Monsoon*, edited by B. Wang, pp. 89–127, Praxis, New York.

Clark, M. P., and M. C. Serreze (2000), Effects of variations in East Asian snow cover on modulating atmospheric circulation over the North Pacific Ocean, *J. Clim.*, *13*, 3700–3710.

Ding, Y. H. (1994), *Monsoons Over China*, 419 pp., Springer, New York.

Gong, D., and S. Wang (1999), Definition of Antarctic Oscillation Index, *Geophys. Res. Lett.*, *26*, 459–462.

Gong, D., S.-W. Wang, and J.-H. Zhu (2001), East Asian winter monsoon and Arctic Oscillation, *Geophys. Res. Lett.*, *28*, 2073–2076.

Gong, G., D. Entekhabi, and J. Cohen (2003), Modeled northern hemisphere winter climate response to realistic Siberian snow anomalies, *J. Clim.*, *16*, 3917–3931.

Hamada, J.-I., M. Yamanaka, J. Matsumoto, S. Fukao, P. Winarso, and T. Sribimawati (2002), Spatial and temporal variations of the rainy season over Indonesia and their link to ENSO, *J. Meteorol. Soc. Jpn.*, *80*, 285–310.

Jhun, J.-G., and E.-J. Lee (2004), A new East Asian winter monsoon index and associated characteristics of winter monsoon, *J. Clim.*, *17*, 711–726.

Ji, L. R., et al. (1997), Model study on the interannual variability of Asian winter monsoon and its influence, *Adv. Atmos. Sci.*, *14*, 1–22.

Jones, P. D. (1987), The early twentieth century Arctic High—Fact or fiction?, *Clim. Dyn.*, *1*, 63–75.

Kanamitsu, M., W. Ebisuzaki, J. Woollen, S.-K. Yang, J. J. Sling, M. Fiorino, and G. L. Potter (2002), NCEP-DOE AMIP-II reanalysis (R-2), *Bull. Am. Meteorol. Soc.*, *83*, 1631–1643.

Kidson, J. W. (1975), Eigenvector analysis of monthly mean surface data, *Mon. Weather Rev.*, *103*, 182–186.

Kumar, A., and F. Yang (2003), Comparative influence of snow and SST variability on extratropical climate in northern winter, *J. Clim.*, *16*, 2248–2261.

Kutzbach, J. E. (1970), Large-scale features of monthly mean Northern Hemisphere anomaly maps of sea-level pressure, *Mon. Weather Rev.*, *98*, 708–716.

Lau, K. M., and C. P. Chang (1987), Planetary scale aspects of winter monsoon and teleconnections, in *Monsoon Meteorology*, edited by C. P. Chang and T. N. Krishnamurti, pp. 161–202, Oxford Univ. Press, New York.

L'Heureux, M. L., and D. W. J. Thompson (2006), Observed relationships between El Nino-Southern Oscillation and the Extratropical zonal-mean circulation, *J. Clim.*, *19*, 276–287.

Li, X. Z. (1955), A study of cold waves in East Asia, in *Offprints of Scientific Works in Modern China—Meteorology (1919–1949)* (in Chinese), edited by X. Z. Li, pp. 35–117, Science Press, Beijing.

Li, J. P., and J. Wang (2003a), A modified zonal index and its physical sense, *Geophys. Res. Lett.*, *30*(12), 1632, doi:10.1029/2003GL017441.

Li, J. P., and J. Wang (2003b), A new North Atlantic Oscillation index and its variability, *Adv. Atmos. Sci.*, *20*(5), 661–676.

Li, J. P., and Q. C. Zeng (2002), A unified monsoon index, *Geophys. Res. Lett.*, *29*(8), 1274, doi:10.1029/2001GL013874.

Li, Y., W. Cai, and E. P. Cambpell (2005), Statistical modeling of extreme rainfall in Southwest Australia, *J. Clim.*, *18*, 852–863.

Lorenz, E. N. (1951), Seasonal and irregular variations of the Northern Hemisphere sea-level pressure profile, *J. Meteorol.*, *8*, 52–59.

Marshall, G. J. (2003), Trends in the Southern Annular Mode from observations and reanalyses, *J. Clim.*, *16*, 4134–4143.

Matsumoto, J. (1992), The seasonal changes in Asian and Australian monsoon regions, *J. Meteorol. Soc. Jpn.*, *70*, 257–273.

Namias, J. (1959), Recent seasonal interaction between North Pacific waters and the overlying atmospheric circulation, *J. Geophys. Res.*, *64*, 631–646.

Namias, J. (1965), Macroscopic association between monthly mean sea-surface temperature and overlying winds, *J. Geophys. Res.*, *70*, 2307–2318.

Nan, S., and J. Li (2003), The relationship between the summer precipitation in the Yangtze River valley and the boreal spring Southern Hemisphere annular mode, *Geophys. Res. Lett.*, *30*(24), 2266, doi:10.1029/2003GL018381.

Nan, S., and J. Li (2005), The relationship between the summer precipitation in the Yangtze River valley and the boreal spring Southern Hemisphere annular mode: The role of the Indian Ocean and South China Sea as an "ocean bridge" (in Chinese), *Acta Meteorol. Sin.*, *63*, 847–856.

Nan, S., J. Li, X. Yuan, and P. Zhao (2008), Boreal spring Southern Hemisphere annual mode, Indian Ocean SST and East Asian summer monsoon, *J. Geophys. Res.*, *114*, D02103, doi:10.1029/2008JD010045.

North, G. R., et al. (1982), Sampling errors in the estimation of empirical orthogonal functions, *Mon. Weather Rev.*, *110*, 699–706.

Ramage, C. S. (1971), *Monsoon Meteorology*, *Int. Geophys. Ser.*, vol. 15, 296 pp., Elsevier, San Diego, Calif.

Rogers, J. C. (1984), The association between the North Atlantic Oscillation and the Southern Oscillation in the Northern Hemisphere, *Mon. Weather Rev.*, *112*, 1999–2015.

Rogers, J. R., and H. van Loon (1982), Spatial variability of sea level pressure and 500 mb height anomalies over the Southern Hemisphere, *Mon. Weather Rev.*, *110*, 1375–1392.

Rossby, C.-G. (1939), Relations between variations in the intensity of the zonal circulation of the atmosphere and displacements of the semipermanent centers of action, *J. Mar. Res.*, *2*, 38–55.

Smith, T. M., and R. W. Reynolds (2004), Improved extended reconstruction of SST (1854–1997), *J. Clim.*, *17*, 2466–2477.

Tao, S. Y. (1957), A study of activities of cold airs in East Asian winter, in *Handbook of Short-Term Forecast* (in Chinese), edited by China Meteorological Administration, pp. 60–92, Meteorology, Beijing.

Thomas, R. A., and P. J. Webster (1994), Horizontal and vertical structure of cross-equatorial wave propagation, *J. Atmos. Sci.*, *51*, 1417–1430.

Thompson, D. W. J., and J. M. Wallace (2000a), Annular modes in the extratropical circulation. Part I: Month-to-month variability, *J. Clim.*, *13*, 1000–1016.

Thompson, D. W. J., and J. M. Wallace (2000b), Annular modes in the extratropical circulation. Part I: Trends, *J. Clim.*, *13*, 1018–1036.

Trenberth, K. E., D. P. Stepaniak, and L. Smith (2004), Interannual variability of patterns of atmospheric mass distribution, *J. Clim.*, *18*, 2812–2825.

Uppala, S. M., et al. (2005), The ERA-40 re-analysis, *Q. J. R. Meteorol. Soc.*, *131*, 2961–3012, doi:10.1256/qj.04.176.

Walker, G. T. (1928), World weather, *Q. J. R. Meteorol. Soc.*, *54*, 79–87.

Wallace, J. M., and D. S. Gutzler (1981), Teleconnections in the geopotential height filed during the Northern Hemisphere winter, *Mon. Weather Rev.*, *109*, 784–812.

Wang, B., and T. Li (2004), East Asian monsoon and ENSO interaction, in *East Asian Monsoon*, edited by C.-P. Chang, pp. 172–212, World Sci., Singapore.

Wang, B., et al. (2008), How accurately do coupled climate models predict the Asian-Australian monsoon interannual variability?, *Clim. Dyn.*, *30*, 605–619.

Watanabe, M., and T. Nitta (1998), Relative impacts of snow and sea surface temperature anomalies on an extreme phase in the winter atmospheric circulation, *J. Clim.*, *11*, 2837–2857.

Watanabe, M., and T. Nitta (1999), Decadal changes in the atmospheric circulation and associated surface climate variations in the Northern Hemisphere winter, *J. Clim.*, *12*, 494–509.

Wu, Z., and J. Li (2008), Prediction of the Asian-Australian monsoon interannual variations with the grid-point atmospheric model of IAP LASG (GAMIL), *Adv. Atmos. Sci.*, *25*(3), 387–394.

Wu, B., and J. Wang (2002), Winter Arctic Oscillation, Siberian High and East Asian winter monsoon, *Geophys. Res. Lett.*, *29*(19), 1897, doi:10.1029/2002GL015373.

Wu, B., R. Zhang, and R. D'Arrigo (2006a), Distinct modes of the East Asian winter monsoon, *Mon. Weather Rev.*, *134*, 2165–2179.

Wu, Z., Z. Jiang, and J. He (2006b), The comparison analysis of flood and droughts features among the first flood period in South China, Meiyu period in the Yangtze River and Huaihe River valleys and rainy season in north China in the late 50 years, *China J. Atmos. Sci.*, *30*(3), 391–401.

Xue, F., H. J. Wang, and J. H. He (2003), Interannual variability of Mascarene High and Australian High and their influences on summer rainfall over east Asia, *China Sci. Bull.*, *48*, 492–497.

Yang, S., K. M. Lau, and K. M. Kim (2002), Variations of the East Asian jet stream and Asian-Pacific-American winter climate anomalies, *J. Clim.*, *15*, 306–325.

Yuan, X., and C. Li (2008), Climate modes in southern high latitudes and their impacts on Antarctic 497 sea ice, *J. Geophys. Res.*, *113*, C06S91, doi:10.1029/2006JC004067.

Zhu, C. W., J. H. He, and G. X. Wu (2000), East Asian monsoon index and its interannual relationship with large-scale thermal dynamic circulation (in Chinese), *Acta Meteorol. Sin.*, *58*, 391–402.

J. Li and Z. Wu, State Key Laboratory of Numerical Modeling for Atmospheric Sciences and Geophysical Fluid Dynamics, Institute of Atmospheric Physics, CAS, P.O. Box 9804, Beijing 100029, China. (ljp@lasg.iap.ac.cn)

X. Liu, National Meteorological Center, China Meteorological Administration, 40 South Zhongguancun Road, Beijing 100081, China.

B. Wang, Department of Meteorology and IPRC, University of Hawaii, 1680 East West Road, Post 40, Honolulu, HI 96822, USA.